Progress In Electromagnetics Research C, Vol. 115, 127–144, 2021

Research on Estimation Method of Information of Multiple Charged Particles Using Electrostatic Sensor Array

Zhirong Zhong[1, 2, *], Hongfu Zuo[1, 2, *], Jiachen Guo[1, 2], and Heng Jiang[1, 2]

Abstract—The electrostatic sensor is a rapidly developing particle monitoring sensor. This paper applies sensor array to inverse the information carried by detected multiple charged particles precisely. It breaks through the constraint that the detailed information of particles cannot be obtained in previous studies. The proposed method can be widely applied to oil line and gas path debris monitoring. The sensing mathematical model and finite-element model are established. A compressive sensing-based method is proposed to invert the information of charged particles. Through simulation and experimental verification, the method can accurately estimate the centroid of multiple particles, the total charge quantity of the particle cluster, the spatial position of each particle, and the charge quantity carried by each particle in the multiple particles with a low error rate when the multiple particles are distributed near the pipe wall of flow channel.

1. INTRODUCTION

As one of the most vital parts of an aircraft, the aero-engine is a complicated system and has extremely high requirements for operational safety. Till now, aero-engine related incidents still occur frequently enough to indicate that the current health management systems still lack sufficient ability for adequate advance warning of faults. Electrostatic monitoring technology for gas paths and oil line in aero-engines is one of the technologies which has the ability to provide new information, more reliable information, and earlier warning information about faults than existing technologies to satisfy the requirement of the PHM (Prognostic and Health Management) ability of an aero-engine [1].

The advantage of electrostatic monitoring technology (EMT) is that it can offer timely warning information about early faults by monitoring the change in the electrostatic level in the gas path or oil line of the aero-engines. It provides a novel method for on-line monitoring and diagnosis for components with rub faults, combustion effectiveness degradation, or wear faults. Such faults as these usually cannot be easily detected by other current monitoring technologies. Thus, electrostatic monitoring technology is a useful additional tool for early detection and progressive monitoring of component deterioration.

Electrostatic monitoring for aero-engine is a promising field. The basic principle of electrostatic monitoring in the field of aero-engine is to monitor the electrification of the charged particles in the gas path or oil line with the help of rod-shaped or ring-shaped electrostatic sensors. The monitored charged particles are usually the direct product of wear, friction, or combustion, such as wear debris, gas path debris, and carbon particles. Moreover, the charged state of the particles can reflect the mode, mechanism and severity of wear, friction, and combustion.

The technology involves monitoring the electrostatic charge to detect debris in the exhaust gas was first discovered by the Air Force Institute in the 1970s [2]. Further research on electrostatic monitoring technology was undertaken at various times by the United Technologies Corporation [3],

Received 22 July 2021, Accepted 1 September 2021, Scheduled 13 September 2021

* Corresponding author: Zhirong Zhong (zhongzhirong2017531@nuaa.edu.cn), Hongfu Zuo (aerodiag@nuaa.edu.cn).

[1] Civil Aviation Key Laboratory of Aircraft Health Monitoring and Intelligent Maintenance, Nanjing University of Aeronautics and Astronautics, Jiangjun Avenue, No. 29, Nanjing 211106, China. [2] College of Civil Aviation, Nanjing University of Aeronautics and Astronautics, Jiangjun Avenue, No. 29, Nanjing 211106, China.

Stewart Hughes Limited (SHL) [4], and Smiths Industries [5, 6]. SHL developed the Engine Distress Monitoring System (EDMS) and Ingested Debris Monitoring System (IDMS), and Powrie et al. proposed a simple electrostatic sensor equation to express the relationship between the measured charge and the real signal, indicating that the sensitivity of the sensor is related to the quantity of the charge and the radial position of the wear debris [7]. Chen et al. established a plate-shaped electrostatic sensor model and analyzed the sensor's sensing characteristics [8–10]. Yan's team at Kent University established various of mathematical model and finite-element model of electrostatic sensor for the physical quantity measurement in pneumatic pipelines [11–13].

Researchers from the University of Southampton first proposed the electrostatic induction method trying to monitor the oil-lubricated gear gluing or adhesive wear [14–16]. Monitoring of the debris, especially the tiny debris, can indicate the onset of failures. Research has shown that in the laboratory the OLS is sensitive to sub 20 μm metallic or nonmetallic debris [17]. Later, the work on electrostatic monitoring technology by SHL and Smiths Industries drove the improvement and application of electrostatic monitoring technology in oil line.

In summary, the existing research is limited to the use of single probe sensor or double probe sensor to investigate the macroscopic characteristic parameters of the induction signal of particle clusters, such as root mean square value, permutation entropy, and kurtosis.

As a particle monitoring sensor, the electrostatic sensor should have the function of directly identifying particles. That's to say, it is typical for an electrostatic monitoring system to obtain the monitored objects' information, such as the number of particles, total charge quantity of particles, and spatial position and charge quantity of each particle. Mao [18] of Nanjing University of Aeronautics and Astronautics has researched the measurement method of multiple wear debris based on compressive sensing (CS) theory. According to the output signal waveform of oil line electrostatic sensor (OLS), the number of wear debris can be identified.

Due to the defect that a single probe sensor cannot provide enough information to solve the specific spatial position and charge quantity of multiple particles, it is natural to use multiple electrostatic electrodes to assemble an electrostatic sensor circular array (ESCA) to solve the specific spatial location and charge quantity of multiple particles. Tang et al. [19] of National Defense University of Science and Technology proposed an array signal processing method based on CS theory focusing on gas path exhaust abnormal debris detecting using a hemisphere-shaped electrostatic sensors' circular array. However, Tang's method is too idealistic in particle reconstruction and has not mentioned how to obtain the charge quantity of particle, and it has not achieved real multi-particle separation, which is not feasible.

In order to study a universal information inversion method suitable for electrostatic monitoring of gas path and oil line, all the monitoring objects in this study are abstracted as charged particles. In addition, the abstract simplification is necessary, reasonable, and acceptable at this degree.

As for identifying particles, this paper is inspired by electrostatic tomography (EST). Meanwhile, there are also significant differences between EST and particle information identification. Specifically, EST usually aims at the densely distributed solid phase in gas-solid two-phase flow, that is, solids can always form a large aggregation area on the observation section. The aero-engine electrostatic monitoring objects are usually very sparse in both space and time and often appear only at a few points of the observation section. For dense solid phase, the least square solution can be obtained by tikhonov regularization, landweber iterative regularization, and other regularization methods when EST is performed. However, for the sparsely distributed charged particles, sparsity is its most significant feature. The sparse solution should be obtained by minimizing the l_0 norm of the constrained solution, that is, the non-zero elements of the solution should be as few as possible.

Compressive sensing (CS) was formally proposed by Donoho [20], Candès [21] and Tao [22] et al. in 2006. The CS theory can be applied to reverse the specific spatial position and charge quantity of a single particle. Meanwhile, it is applied to inverse the total charge quantity of multiple particles innovatively. Out of the accurate result of estimating spatial position and charge quantity of a single particle, a method of multiple particles separation and recognition based on clustering is proposed.

The left sections are organized as follows. Methodology of information inversion is introduced in Section 2. A finite-element model of the ESCA-based particle monitoring system is built and simulated in Section 3. Details of experimental verification are introduced in Section 4. The main results and discussion of results are elaborated in Section 5. Final conclusion are concluded in Section 6.

2. METHODOLOGY OF INFORMATION INVERSION

In this paper, considering the need to balance the number of independent measurements and signal strength, the sensor array with 8 electrodes, which is called ESCA, is selected as an optimized example to analyze [23]. When a single particle passes through the observation cross-section, the theoretical model is established. This means that a mathematical model of the case, when multiple particles pass through the observation cross-section, can be derived from the established theoretical model. Same as the principle of electrostatic tomography, although the 8 electrodes can provide 8 independent measures to the maximum, which is far less than the unknowns. Considering this situation, CS theory is introduced to solve this problem.

2.1. The Structure and the Measurement System of ESCA

As shown in Fig. 1, the ESCA is mainly composed of 8 sensing electrodes, a shield cover isolation layer, and flange. Among them, sensing electrodes are made of cooper, shield cover made of aluminum alloy, and the isolation layer made of ceramics and epoxy. Moreover, an arc-shaped electrode is designed to be with a polar angle of $\pi/18$, and the area between two electrodes is an arc-shaped area with a polar angle of $\pi/36$. The observation cross-section is defined as XOY coordinate plane. Meanwhile, the Z-axis is located at the axis of ESCA which is perpendicular to the XOY plane at the center of the XOY plane. The sensing electrodes are sequentially numbered in counterclockwise order from 1 to 8.

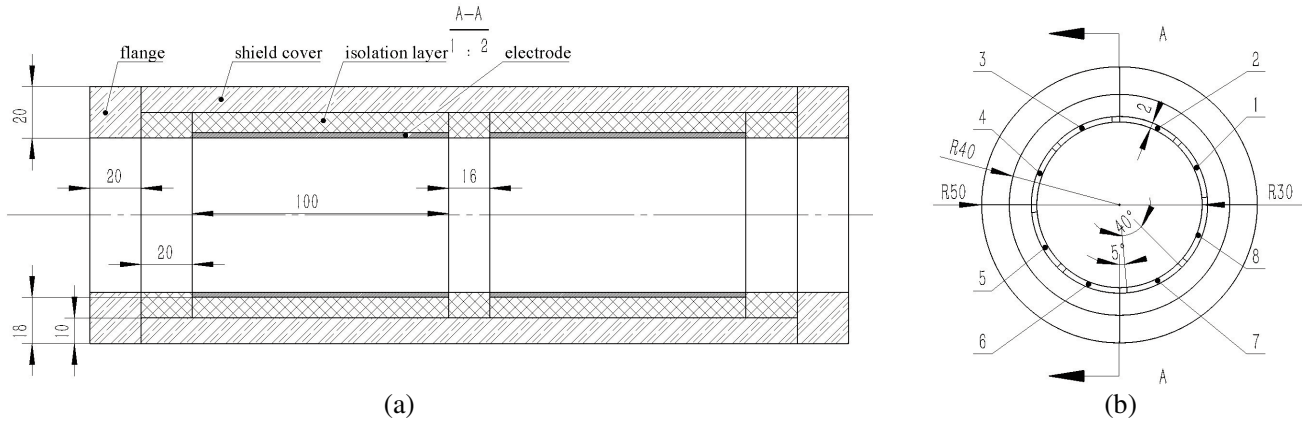

Figure 1. The structure of ESCA: (a) front view and (b) top view.

The electrostatic monitoring system based on ESCA is designed as shown in Fig. 2, and 8 independent measurements can be acquired from 8 sensing electrodes which are independent of each other by the isolation of the isolation layer. In the actual measurement circuit, the output signal of the measurement system is voltage signal, which is the consequence of the signal conditioning circuit. Multiply the voltage signal by the feedback capacitor of the signal conditioning circuit to obtain the induced charge signal sensed by the electrodes.

2.2. Sensing Mathematical Model and Simulation

2.2.1. Sensing Mathematical Model

To understand the characteristics of ESCA, the relationship between the particle charge and the sensing charge needs to be further studied, which can be easily obtained by establishing the ESCA's mathematical model. According to the superposition principle, the case of multiple particles passing through can be equivalent to that of single particle, so the model in this paper is established only for the case of single particle and given that the particle can be modeled as a point charge. Out of the symmetry and similarity of the electrodes located in ESCA, focus on modeling a single electrode can be easily extended to the whole electrode array.

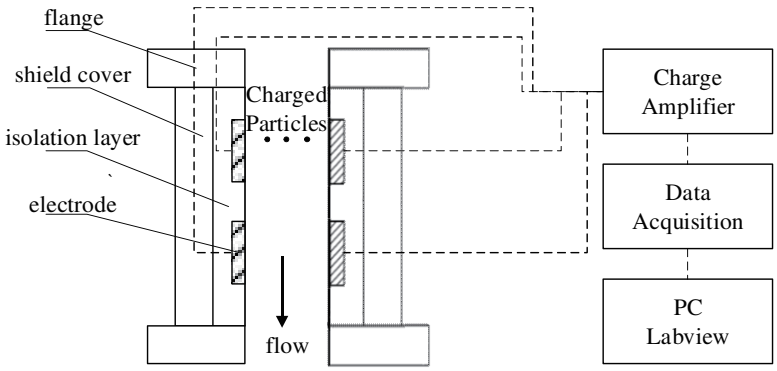

Figure 2. The electrostatic monitoring system.

Assuming that the charge of the particle is q, and the equivalent point charge is located at a position deviating from the Z axis at a distance of ρ ($0 \leq \rho < R$, where R represents the radius of ESCA), that is, the radial position of the point charge on the cross-section is ρ, located at the position of the polar angle φ with the positive X-axis. Furthermore, the point charge is located at position z on the Z-axis. Set a certain electrode located at the position sandwiched by polar angles θ_0 and θ_1. The length of electrodes is $2l$ at Z direction, which are divided equally by the XOY plane. Then transform Cartesian coordinates to cylindrical coordinates. In the XOY plane, the point charge is located at the position of (ρ, φ, 0). Take a microelement sensing area ds on the electrode that intersects the XOZ plane, and its position coordinates can be expressed as (R, θ, z), where $\theta_0 \leq \theta \leq \theta_1$. The relative position of the point charge and the electrode is shown in Fig. 3.

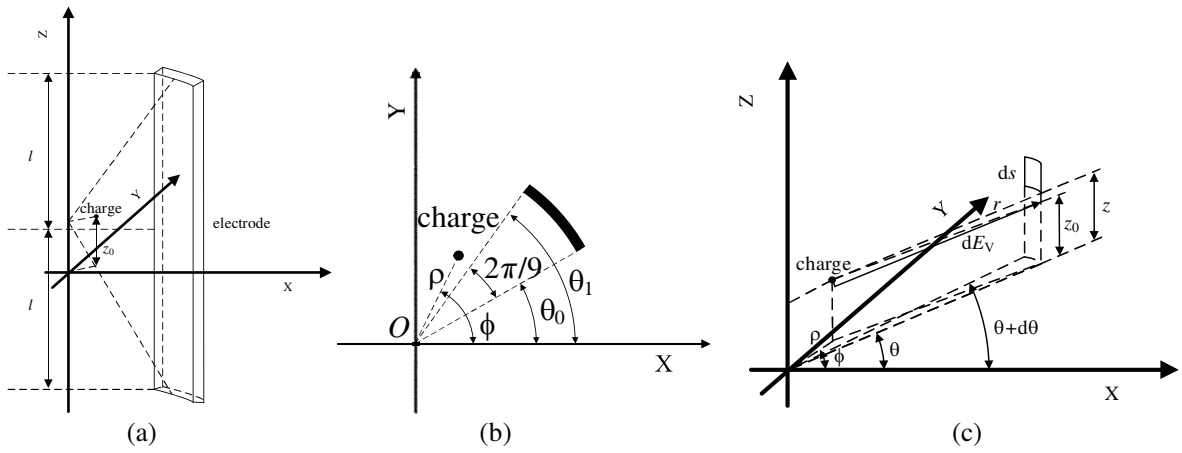

Figure 3. The relative position of the point charge and the electrode: (a) front view, (b) top view and (c) Schematic diagram of ESCA model cylindrical coordinates.

According to Coulomb's theorem and Gauss' theorem, the induced charge Q_s on an electrode can be obtained by Eq. (1). Among them, $q_{particle}$ is the charge quantity of a point charge.

$$Q_s = -\frac{q_{particle}}{4\pi} \int_{\theta_0}^{\theta_1} d\theta \int_{-l}^{l} \frac{R^2 - \rho R \cos|\theta - \varphi|}{\left(R^2 + \rho^2 - 2R\rho\cos|\theta - \varphi| + (z - z_0)^2\right)^{\frac{3}{2}}} dz \tag{1}$$

Equation (1) is the mathematical model of a single electrode sensing. Based on the built mathematical model, it is easy to infer the mathematical model of the entire ESCA considering all electrodes. Obviously, when the number of particles is k, the induced charge $Q_s(i)$ on ith ($0<i \leq 8$) electrode can be described by Equation (2). $\varphi(n)$ represents the polar angle of nth particle relative to

the positive direction of the X axis; $\rho(n)$ means the ρ value of the nth particle position; and $q_{particle}(n)$ is the charge quantity of the nth particle in k particles, which means $0<n \leq \quad k$.

$$Q_s(i) = -\sum_{n=1}^{k} \frac{q_{particle}(n)}{4\pi} \int_{\theta_0+\frac{\pi}{4}(i-1)}^{\theta_1+\frac{\pi}{4}(i-1)} d\theta \int_{-l}^{l} \frac{R^2 - \rho(n) R\cos|\theta - \varphi(n)|}{\left(R^2 + \rho(n)^2 - 2R\rho(n)\cos|\theta - \varphi(n)| + (z-z_0)^2\right)^{\frac{3}{2}}} dz \quad (2)$$

Generally speaking, the sensing characteristics of the ESCA can be understood by spatial sensitivity distribution. Spatial sensitivity distribution represents the relationship among the induced charge on electrodes, the particle charge, and the particle position. Define the spatial sensitivity as Equation (3)

$$S(i) = \frac{Q_s(i)}{q_{particle}} = -\frac{1}{4\pi} \int_{\theta_0+\frac{\pi}{4}(i-1)}^{\theta_1+\frac{\pi}{4}(i-1)} d\theta \int_{-l}^{l} \frac{R^2 - \rho R\cos|\theta - \varphi|}{\left(R^2 + \rho^2 - 2R\rho\cos|\theta - \varphi| + (z-z_0)^2\right)^{\frac{3}{2}}} dz \quad (3)$$

2.2.2. Numerical Simulation

In this paper, the entire observation section is discretized into multiple points, and the sensitivity numerical solution is solved to form a sensitivity matrix S mapped by point positions. The Distmesh toolkit is used to mesh the observation cross-section of ESCA.

As shown in Fig. 4, the circular area in the XOY plane is discretized into a grid with 347 grid points. By applying numerical simulation, a spatial sensitivity distribution matrix S with a dimension of 8×347 can be obtained.

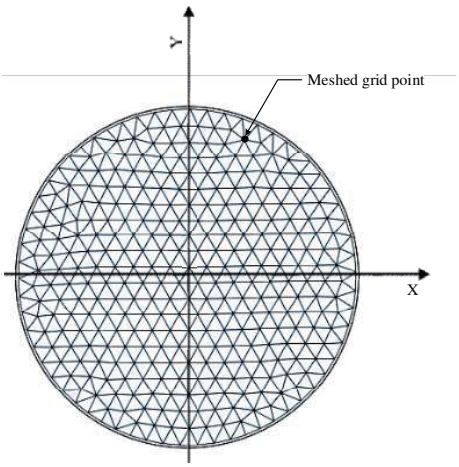

Figure 4. The meshed observation cross-section.

2.3. Particle Information Inversion Algorithm

2.3.1. Compressive Sensing Theory Basis

CS theory treats a sparse signal to be measured as an N-dimensional sparse vector x. In signal acquisition, CS theory uses an $M \times N$-dimensional ($M << N$) sensing matrix Θ to directly compress x into an M-dimensional measurement vector y as shown in Equation (4). This compression process can retain enough information to reconstruct the sparse vector x under certain conditions, and then only need to solve a sparse optimization problem to accurately reconstruct x from y precisely.

$$y = \Theta x \quad (4)$$

In Eq. (4), the sensing matrix Θ satisfying restricted isometry property (RIP) is a necessary condition for x to be uniquely reconstructed correctly. In this paper, the numerical solution of sensitivity can be obtained by using discrete mathematical simulation, so Eq. (3) can be transformed into Eq. (5),

where Q_s is a vector consisting of M measurements $Q_s(i)$; S represents the sensitivity matrix of ESCA in the XOY plane; and q is a vector which consists of the information of induced charge distribution. In addition, the sensitivity reveals the inherent connection between charged debris and the quantity of charge induced by the electrode, which is a kind of vital link.

$$Q_s{=}Sq \tag{5}$$

Before reconstruction, the method based on singular value decomposition (SVD) is adopted to preprocess Eq. (5), so that the processed sensing matrix S_{svd} in the equation satisfies the RIP condition. The data preprocessing algorithm is as follows.

Algorithm 1 Data preprocessing algorithm

Step 1: Decompose S as $S = U[\Delta 0]V^T$. $\Delta = \mathrm{diag}(\delta_1, \delta_2, \ldots, \delta_M)$, where $\delta_1 \geq \delta_2 \geq \ldots \geq \delta_M > 0$ are all M singular values of S
Step 2: Let $\Delta* = \mathrm{diag}(1/\delta_1, 1/\delta_2, \ldots, 1/\delta_M)$ and $Z = [I\,0]V^T$, then $Q_{ssvd} = Zq$
Step 3: Unitize each column of Z, and use the resulting matrix as the processed sensitivity matrix S_{svd}. Thus $S_{svd} = Z \cdot \mathrm{diag}(1/||z_1||_2, 1/||z_2||_2, \ldots, 1/||z_n||_2)$, where $z_1, z_2, \ldots, z_n$ are the column vectors of Z.
Step 4: Define $q_{svd} = \mathrm{diag}(||z_1||_2, ||z_2||_2, \ldots, ||z_n||_2) \cdot q$. Then $Q_{ssvd} = S_{svd} \cdot q_{svd}$

In theory, l_0-minimization is an ideal constraint to figure out a group of sparse solutions which have the fewest nonzero elements. However, solving l_0-minimization directly is a non-deterministic polynomial hard (NP-hard) problem. It is believed that in some situations the l_0-minimization problem can be transformed into an l_1-minimization one as Eq. (6). The l_1-minimization is a typical convex optimization problem, and it is easy to solve by using interior point method. Among them, the primal-dual interior point method is often more effective than the barrier function method, especially where high precision is required. Therefore, q_{svd} can be correctly inversed by using the primal-dual interior point method.

$$\hat{q}_{svd} = \arg\min_{q_{svd}} \|Q_{ssvd} - S_{svd}q_{svd}\|_1 \tag{6}$$

2.3.2. Centroid Position and Total Charge Quantity Inversion Algorithm of Multiple Particles

Out of the superposition principle, it is apparent that multiple particles can be equivalent to a single equivalent particle when passing through. This particle is defined to be an equivalent particle, which means that its charge quantity equal to the total charge quantity of multiple particles and its position represents the position of the centroid of particles according to the charge quantity. In a sense, an equivalent particle can describe the overall position and charge quantity information of the multiple particles. Thus, the total charge quantity of multiple particles can be obtained by calculating the charge quantity of the equivalent particle, which means that the problem is transformed into a single particle information inversion problem. In conclusion, the total charge quantity of multiple particles can be obtained by applying the method as Algorithm 2.

Algorithm 2 Information estimation method of multiple particles

Step 1: Using proposed data preprocessing algorithm to get Q_{ssvd} and S_{svd}
Step 2: Using the primal-dual interior point method to solve Equation (6), q_{svd} is calculated.
Step 3: Calculate $q = \mathrm{diag}(1/||z_1||_2, 1/||z_2||_2, \ldots, 1/||z_n||_2) \cdot q_{svd}$
Step 4: Obtain the estimated spatial position of multiple particles centroid by (7), where (x_n, y_n) are the position of discrete point correspond to nth column of S
Step 5: Calculate the inversed total charge quantity q_{total} by (8), where M is the number of probes

$$(\hat{x}, \hat{y}) = \left(\sum_{n=1}^{N} x_n q_n \Big/ \sum_{n=1}^{N} q_n, \sum_{n=1}^{N} y_n q_n \Big/ \sum_{n=1}^{N} q_n,\right) \tag{7}$$

$$q_{total}=-\sum_{i=1}^{M}4\pi Q_s\left(i\right)\Bigg/M\int_{\theta_0+\frac{\pi}{8}(i-1)}^{\theta_1+\frac{\pi}{8}(i-1)}d\theta\int_{-l}^{l}\frac{R^2-\rho R\cos\left|\theta-\varphi\right|}{\left(R^2+\rho^2-2R\rho\cos\left|\theta-\varphi\right|+\left(z-z_0\right)^2\right)^{\frac{3}{2}}}dz \tag{8}$$

2.3.3. Estimation Method for the Spatial Position and Charge of Each Particle in the Multi-Particle

The problem of estimating spatial position and charge quantity of each particle of multiple particles can be described as Eq. (9). In Equation (9), $p(n,\, i)$ is the sensitivity of the nth particle in the particle cluster relative to the ith probe.

$$\begin{aligned}
&\left[Q_s\left(1\right)\ldots Q_s\left(8\right)\right]^T=\begin{bmatrix} p(1,1)\ldots p(k,1) \\ \vdots \quad \vdots \quad \vdots \\ p(1,8)\ldots p(k,8) \end{bmatrix}\cdot\left[q_{particle}(1)\ldots q_{particle}(k)\right]^T \\
&p(n,i)=-\frac{1}{4\pi}\int_{\theta_0+\frac{\pi}{4}(i-1)}^{\theta_1+\frac{\pi}{4}(i-1)}d\theta\int_{-l}^{l}\frac{R^2-\rho\left(n\right)R\cos\left|\theta-\varphi\left(n\right)\right|}{\left(R^2+\rho\left(n\right)^2-2R\rho\left(n\right)\cos\left|\theta-\varphi\left(n\right)\right|+\left(z-z_0\right)^2\right)^{\frac{3}{2}}}dz \\
&s.t.\quad \sum_{n=1}^{k}q_{particle}(n)-q_{total}=0\qquad q(n)>0
\end{aligned} \tag{9}$$

According to the principle of superposition, the charge distribution vector $q_{multiple}$ retrieved when there are multiple particles should be equal to the sum of the distribution vector retrieved when each particle in the multiple particles passes through the observation section alone. But in fact, the position and charge information of each particle in the multiple particles are unknown variables which we actually need to solve. That is, their distribution vector cannot be directly obtained. To solve this problem, a method by setting many candidate particles to separate particles' information from $q_{multiple}$ is proposed. The details of the method are as follows.

Select all 347 mesh grid points as shown in Fig. 4 to be all possible positions of candidate single particle, and place a single point charge of +1C on all 347 points respectively to perform 347 times of single test. Hence, 347 candidate single particle charge distribution vectors can be obtained, and it can also be said that in these vectors actually each candidate corresponds to a single particle. According to the sequence number, 91 vectors form matrix D of 347×347 called the candidate particle inversion dictionary. The relationship between $q_{multiple}$ and D can be constructed as Equation (10), where p_w represents the position weight vector among candidate particles.

$$p_w=q_{multiple}/D \tag{10}$$

It is necessary to filter the weights in p_w and eliminate the outliers in the weight vector according to the pauta criterion. This process can be expressed by Equation (11). In Equation (11), p_{wp} marks the preprocessed weight vector, and μ and σ represent the mean and standard deviation of p_w, respectively. Meanwhile, c is an empirical parameter, and the value in this paper is determined to be 0.5 based on the experience.

$$\operatorname{sgn}\left(x\right)=\begin{cases}1, & x>0\\ 0 & x\le0\end{cases}\quad p_{wp}=\operatorname{sgn}\left(p_w-\left(\mu-c\cdot\sigma\right)\right)\cdot\left(p_w-\left(\mu-c\cdot\sigma\right)\right) \tag{11}$$

In particular, the number of particles is known in simulations and experiments, but the number of particles in the cross-section observed in the actual industrial environment is unknown. However, some studies have basically solved the problem of using electrostatic sensors to measure the number of particles. For example, Armour-Chelu et al. [24] proposed a signal processing method of the data from the probes to reveal density information about the flow of particles in a pipeline; Hussain et al. [25] investigated a method to detect the charge polarity and the density of oppositely charged materials; Mao [18] proposed a CS based method that can accurately identify the number of wear debris when multiple wear debris pass through the sensor at the same time. This paper applies Mao's method to calculate the number of multiple particles, which makes this research applicable to the actual oil line of aero-engine. Since most of the particles inhaled by the inlet of aero-engine are particle clusters with

hundreds of particles; the existing method for determining the number of particles is not suitable for such a large number of particle clusters; and the number of probes is limited, the application on the gas path requires further breakthroughs.

From the distribution results of p_{wp}, it can be considered that when the number of particles is k, it is reasonable to divide the weights corresponding to all candidate particles into k categories. Among them, the distance in the three-dimensional feature space F composed of plane coordinates (x, y) and p_{wp} between candidate particles needs to be used as the basis for classifying candidate particles into a certain class. Candidate particles classified into the same class will be reconstructed into single particles according to the corresponding weights. That is, the plane positions of k particles are finally reconstructed as the final output. From the above analysis, it is natural to apply a clustering method to classify candidate particles in the feature space $F(x, y, p_{wp})$.

Fuzzy c-means (FCM) algorithm is applied to clustering. FCM was developed by Dunn [26]. The FCM algorithm attempts to partition a finite collection of n elements $X = \{x_1, \ldots, x_n\}$ into a collection of c fuzzy clusters with respect to some given criteria. Given a finite set of data, the algorithm returns a list of c cluster centers $C = \{c_1, \ldots, c_c\}$ and a partition matrix. Define $W = w_{i,j} \in [0, 1]$, $i = 1, \ldots, n$, $j = 1, \ldots, c$, where each element $w_{i,j}$ represents the degree to which the element x_i belongs to the clusterc_j. The FCM aims to minimize the objective function as Equation (12).

$$\underset{C}{\operatorname{argmin}} \sum_{i=1}^{n} \sum_{j=1}^{c} w_{ij}^{m} \left\| x_i - c_j \right\|^2, w_{ij} = 1 \Bigg/ \sum_{k=1}^{c} \left(\|x_i - c_j\| / \|x_i - c_k\| \right)^{2/m-1} \tag{12}$$

By applying FCM, the candidate particles can be clearly divided into k clusters. Next, the jth particle in the multi-particle is reconstructed from the jth candidate particles cluster by means of the centroid weighting method. By the way, the spatial position of the jth particle can be estimated by Equation (13).

$$\left(\hat{x}^j, \hat{y}^j\right) = \left(\sum_{n=1}^{N^j} x_n^j p_{wp}^j \Bigg/ \sum_{n=1}^{N^j} p_{wp}^j, \sum_{n=1}^{N^j} y_n^j p_{wp}^j \Bigg/ \sum_{n=1}^{N^j} p_{wp}^j \right) \quad s.t. \quad \sum_{j=1}^{k} N^j = N, \quad 1 \le j \le k \tag{13}$$

It is worth noting that when k is less than the number of sensing electrodes, Equation (13) is over determined and can be solved to obtain the least square solution as the final charge quantity estimate value. When k is exactly equal to 8, Equation (13) is exactly determined, and Equation (14) can be derived from Equation (13) to obtain the final estimated value of each particle. When k equals more than 8, the problem is an ill-conditioned problem and can be estimated using such as Tikhonov regularization method with relatively lower accuracy rate to be not discussed temporarily, and it will be considered to be improved in subsequent research. Thus, the upper limit of the resolution of the number of particles in this algorithm is equal to the number of probes.

$$\left[q_{particle}(1), \ldots, q_{particle}(k)\right]^T = \begin{bmatrix} p(1,1) \ldots p(k,1) \\ \vdots \quad \vdots \quad \vdots \\ p(1,8) \ldots p(k,8) \end{bmatrix}^{-1} \cdot \left[Q_s(1), \ldots, Q_s(8)\right]^T \tag{14}$$

3. FINITE ELEMENT MODELING AND SIMULATION

It is difficult to control multiple particles with a measurable charge quantity through the observation cross section at the same time by means of experiment. In this paper, the finite element simulation method is used to simulate the situation of particles with different charge quantities at multiple different test points passing through the observation section to carry out the simulation verification of Algorithm 2.

3.1. Finite Element Modeling

The finite-element model of ESCA is established by using COMSOL multiphysics simulation software. Parametric modeling is adopted, the main size parameters of the solid model are shown in Fig. 1. In

addition, all parameters used in the model are established under the MMGS unit system standard. The particles were modeled as with a sphere of 0.3 mm in radius, which is charged equally on surface.

According to the actual physical process, the physical properties of the model are set as follows: the shield cover is grounded; the electrode is equipotential; the internal space of the tunnel is oil with a relative permittivity of 2.35; and the isolation layer is an insulating ceramic with a relative permittivity of 6. The initial potential everywhere in the model is zero by default, and the two ends of the flange are zero potential by default. The Dirichlet boundary condition $B(P)$ can be described as Equation (15).

$$B(P) = \beta\phi(x, y, z)|_{(x,y,z)\in\Gamma_e,\Gamma_s} \tag{15}$$

where ϕ is the potential generated by charged particle; Γ_e and Γ_s are the boundaries of electrodes and shield cover, respectively; β is a non-zero constant; P is a point on boundary.

The finite-element meshing adopts the method of freely dividing the tetrahedron. In order to ensure the accuracy of the finite-element simulation, the method of controlling the maximum size of the mesh is used to refine the mesh near the surface of the charged particles and the electrodes. The total number of divided grids is 260791. The established model effect is as shown in Fig. 5.

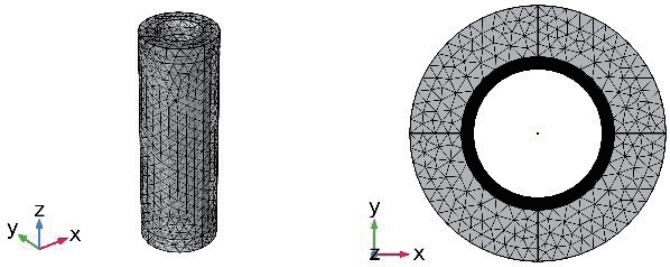

Figure 5. The established finite element model.

3.2. Finite Element Simulating

Perform a finite element simulation on the discrete points shown in Fig. 4. Through the comparison between Fig. 6(a) and Fig. 6(b), it can be known that the sensitivities calculated by numerical simulation and finite element simulation are similar. The error results in Fig. 6(c) show that the absolute error between the finite element simulation and mathematical model simulation results is within 5%, and the error is within the acceptable range. Compared with the boundary conditions of the mathematical

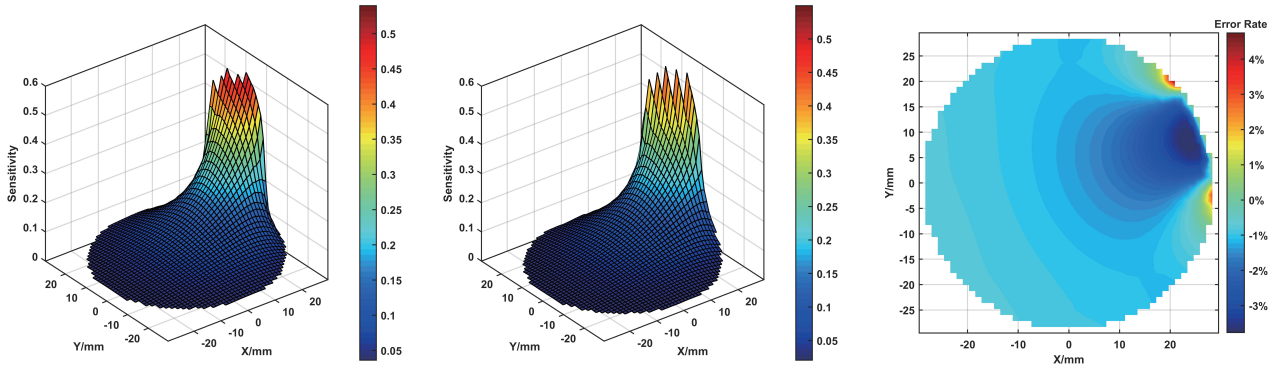

(a) (b) (c)

Figure 6. Sensitivity surface graph of probe 1 calculated by (a) numerical simulation and (b) finite element simulation. (c) The difference between the sensitivity calculated by finite element model and the mathematical model.

model, the finite element simulation is closer to reality. The mathematical model is very ideal, so there are some errors in the value. The correctness of the built finite element model and mathematical model is cross-verified. The simulation data can be used for subsequent algorithm verification.

In this paper, 91 test points are obtained by using equidistant sampling in the observation section.Test points are marked by asterisk and numbered as shown in Fig. 7. In these test points, a number of random test point combinations of 2, 3, and 4 are selected respectively. Subsequently, particles with a random charge between 0 and 1C are placed on the selected test points, and the finite element simulation test is carried out.

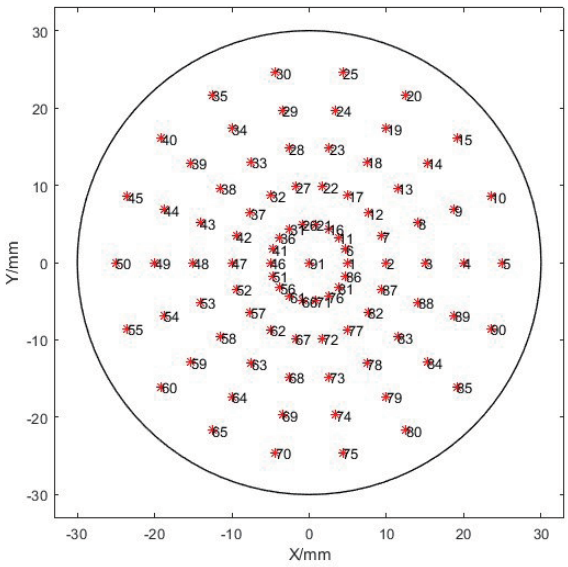

Figure 7. The distribution of selected test points.

4. EXPERIMENT

In Section 4, the oil drop calibration test bench is used to simulate the sensing of the sensor when multiple charged particles pass through the observation section at the same time. The experiment in this section is to verify the effectiveness of the method for estimating the spatial position and charge quantity of each particle among multiple particles.

4.1. The Test Rig

As shown in Figs. 8(a) and 8(b), the test rig [27–29] consists of an oil drop generation and charge section, a sensor support and positioning section, an electrostatic signal acquisition section, and an oil drop charge measurement section. The oil droplet charge section mainly includes oil tank, valve, multi-tubes metal needle, ring electrode, two-axis plane position adjustable platform, and DC adjustable power supply.

When the device works, through the valve the lubricating oil in the oil tank enters the high voltage electric field formed by the multi-tube metal needle and the annular electrode. Under the action of the high voltage electric field, the oil droplets will carry a certain amount of charge. The high voltage electric field strength can be adjusted by the adjustable DC power supply, whose maximum output voltage is 500 V. The relationship between the charge of the oil droplets and the applied voltage can be expressed by the formula: $Q_{oil} = C$, where C is the capacitance of the oil droplets, U the applied voltage, and it is obvious that the charge quantity $_{oil}$ of the oil droplets is proportional to the voltage U. By the way, since the length and diameter of each needle tube of the multi-tube needle used are the same, it can be considered that the size of each oil droplet and the charge quantity on each of the multiple oil droplets dropped each time are equivalent.

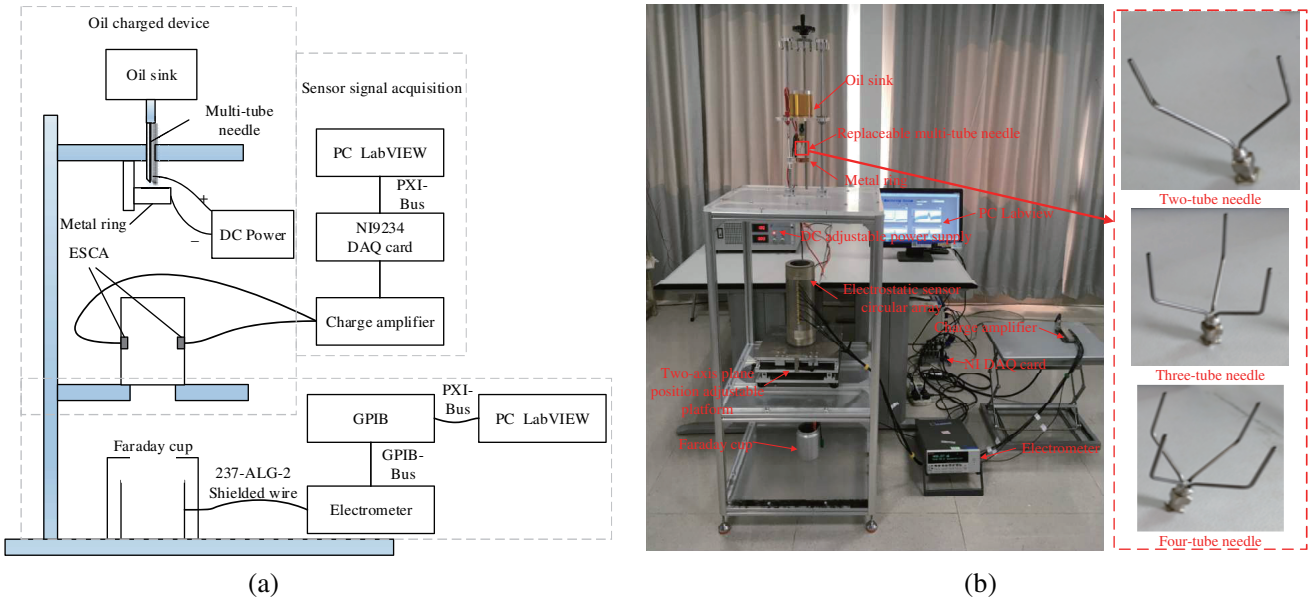

(a) (b)

Figure 8. The calibration test rig: (a) the schematic diagram of calibration test rig (b) the actual calibration test rig and the replaceable multi-tube needles.

Therefore, the test rig can adjust the charge through changing the voltage linearly. The sensor support and position section can accurately adjust the relative position between the ESCA and the drop path of the oil droplets drop through the slide rail and also the altitude of the sensor to adjust the speed when the oil drops pass through the sensor. The output signal of the ESCA can be obtained in real time with NI acquisition card in the signal acquisition section. The charge measurement section measures the exact charge of the oil droplets by means of a Faraday cup and a Keithley 6517B electrometer with a resolution up to 0.01 pC.

4.2. Experimental Design

As shown in Fig. 8(b), the experiment uses 3 types of multi-tube needles with 2, 3, and 4 needle tubes to perform multiple repeated experiments respectively, and the distances between the needle tubes of the multi-tube needles with different numbers of needle tubes are respectively 36 mm, 30 mm, and 25 mm. At this time, keep the different multi-tube needles installed in the same initial centered position, where the center of the sensor and the multi-tube needle are aligned on the Z axis, to ensure that the multi-tube needles' position relative to the sensor does not change. In addition, different voltages were applied to the oil drop generation and charge device to produce oil droplets with different charges. The voltage increased from 0 to 500 V with the step 100 V. The equivalent speed of the oil droplets was set to 3.28 m/s. The purpose of this experiment is to verify that the charged oil droplets produced by the experimental device are proportional to the applied voltage. The output of the Faraday Cup is shown in Fig. 11(a).

Keep the equivalent speed of the oil droplets at 3.28 m/s. When the number of needle tubes of multi-tube needles is set to $m(m = 2, 3, 4)$ and the multi-tube needle has been located in the initial centered position, increase the voltage from 100 V to 500 V with the step 100 V. Then, as shown in Fig. 9(a), rotate the ESCA around the central axis by the angle γ ($\gamma = 0.0873, 0.2618, 0.4363, 0.6109, 0.7854$ rad) counterclockwise, where γ is the angle between the X axis of ESCA after rotation and the X axis of the initial position ($\gamma = 0$, $\Delta = 5$ mm). After traversing all possible values of γ, restore ESCA to the initial position. The next step is to translate the ESCA to the positive X axis direction of the initial position by Δ ($\Delta = 5, 10$ mm). Similarly, rotate ESCA again. Perform the above operation to traverse all possible Δ values. So far, one round of experiments when the number of needle tubes is taken as m is completed. Next, reinstall different multi-tube needles, and conduct a new round

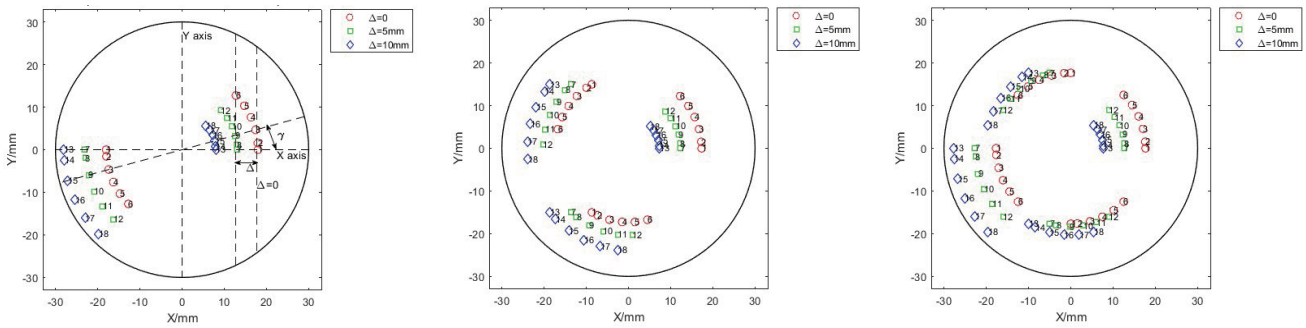

Figure 9. The position distribution of multiple oil droplets when using multi-tube needles: (a) the position distribution of double oil droplets when using a two-tube needle (b) the position distribution of three oil droplets when using a three-tube needle (c) the position distribution of four oil droplets when using a four-tube needle.

of experiments to perform all possible values of m. Just as shown in Fig. 9, it shows all theoretical experiment positions of multiple oil droplets when using 3 types of multi-tube needles. The position distribution of multiple oil droplets is believed to be the actual positions of multiple oil droplets when conducting experiments. So, the position of the oil droplet in Fig. 9 and the charge quantity shown in Fig. 11 are used to verify the accuracy of the oil droplets' position and charge quantity estimated by using the method proposed in this paper. What needs further explanation is that the rotational symmetry of ESCA in the radial direction is taken into consideration, and the position of oil droplets tested by the oil drop test is representative, which can roughly describe the characteristics of all typical positions on the full observation cross-section of ESCA.

5. RESULTS AND DISCUSSION

5.1. Verification of Centroid Position and Total Charge Quantity Inversion Algorithm

It can be seen from Table 1 and Fig. 10 that the total charge quantity of multiple particles can be accurately inverted using the proposed method, and the absolute error rate of inversion using this method is less than 3%. Therefore, it can be considered that the total charge quantity obtained by the inversion is the true value, and the total charge quantity q_{total} can be used as a known condition to determine the charge quantity of a single particle in the particle cluster.

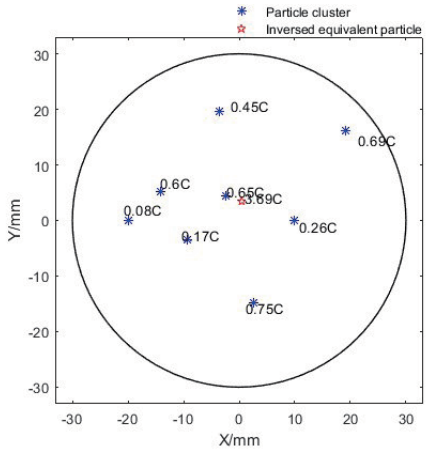

Figure 10. The effect of total charge quantity inversion based on simulated data.

Table 1. The result of total charge quantity inversion based on simulated data.

Test points	Charge quantity of each particle/C	Theoretical total charge quantity/C	Inversion result/C	Error rate/%
64,87	1.00,1.00	2.00	2.02	1.00
24,45	0.86,0.72	1.58	1.62	2.53
19,15	0.37,0.86	1.23	1.20	−2.43
63,58	0.14,0.08	0.22	0.22	0
47,25,22,82	0.91,0.60,0.37,0.60	2.48	2.50	0.96
61,82,8,50	0.43,0.62,0.56,0.23	1.84	1.85	0.80
10,1,6,30	0.78,0.34,0.62,0.99	2.73	2.77	1.31
59,50,22,68,81,79	0.60,0.65,0.92,0.43,0.29,0.63	3.52	3.57	1.55
27,57,5,91,19,56	0.35,0.72,0.03,0.07,0.93,0.09	2.19	2.20	0.64
31,48,23,50,72,48,85,14	0.42,0.28,0.60,0.04,0.06,0.32,0.10,0.17	1.99	2.01	1.01

5.2. Verification of the Estimation Method for the Spatial Position and Charge of Each Particle in the Multi-Particle

The marked points in Fig. 11 represent the measured data points, and the lines are the fitting curves. It was proven from the fitting curves in Fig. 11(b) that the charge of each oil droplet produced by the device was proportional to the applied voltage, which was consistent with the theoretical model.

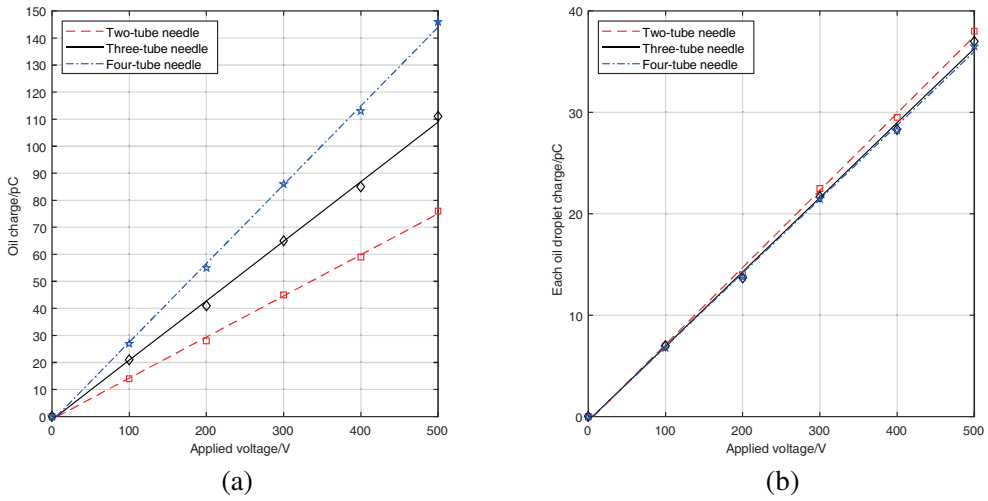

Figure 11. (a) The relationship between the oil droplets charge and the applied voltage and (b) the relationship between each oil droplet charge and the applied voltage.

The experimental data obtained in Section 4 are used to verify the proposed multiple particles inversion algorithm. The error rate of position estimation is defined as the Euclidean distance between the inversion position and the actual position divided by the maximum possible error distance, in which the maximum possible error distance is the inner diameter of ESCA.

As shown in Fig. 12, the actual position and inversed position of multiple particles are marked by asterisk and circle, respectively. The position error rate of each particle inversion is marked by text in the actual position of the particle. In Table 2, the second column refers to the theoretical value of the

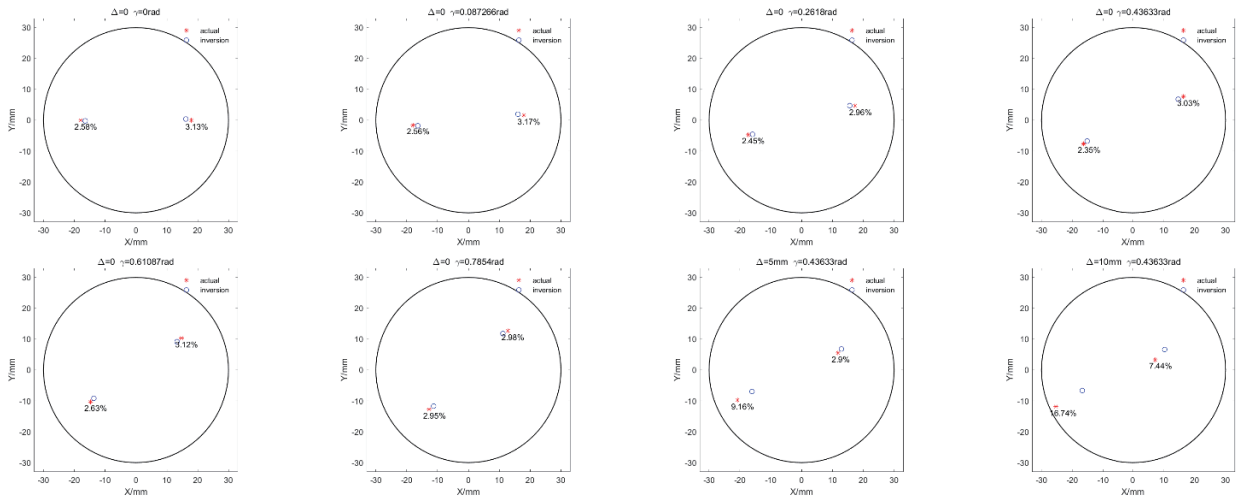

(a)

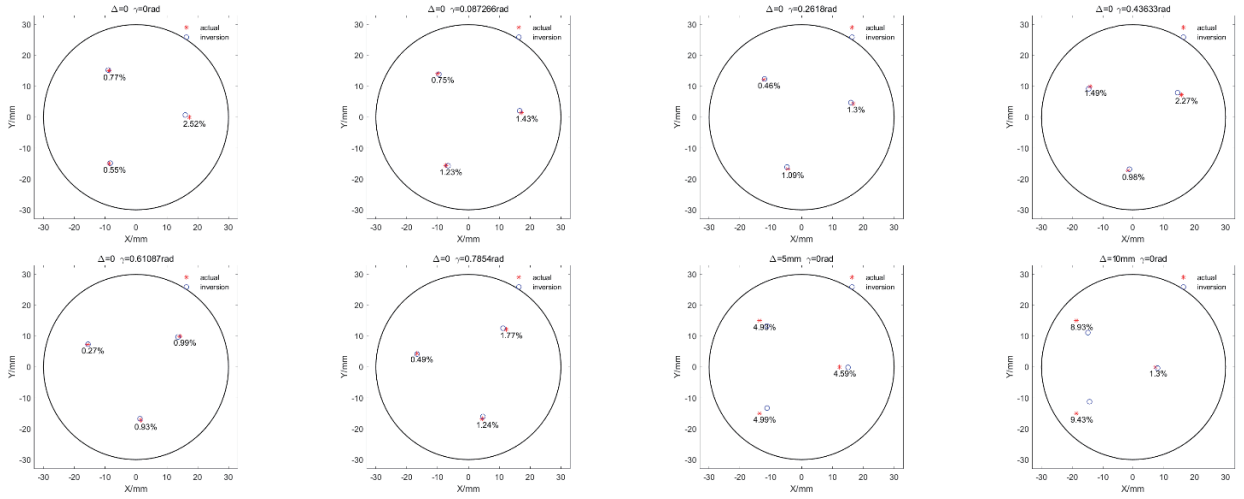

(b)

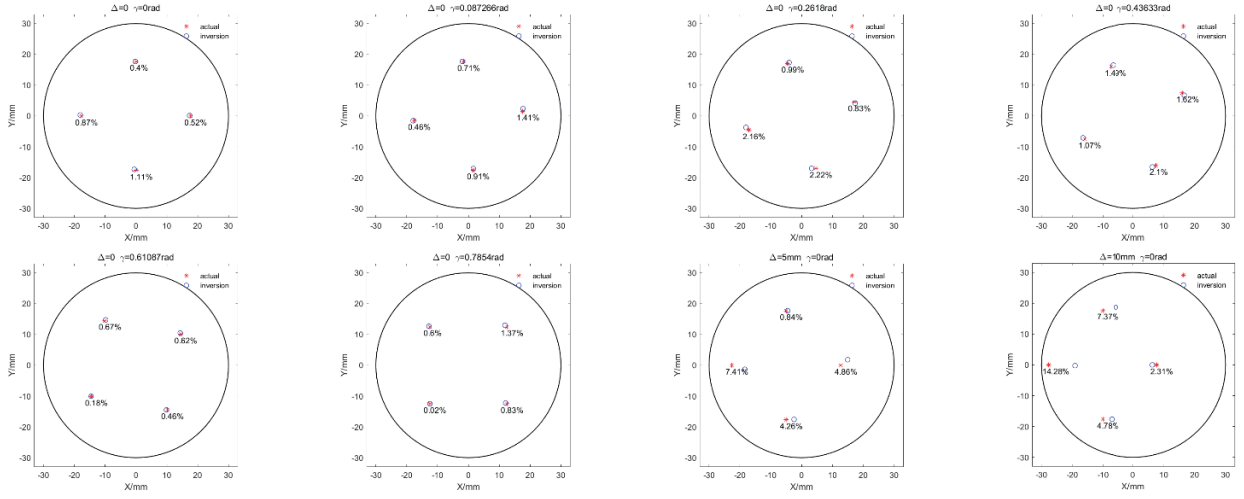

(c)

Figure 12. The effect of estimating the spatial position of multiple particles based on experimental data when the number of needle tubes of the multi-tube needles (a) $m = 2$ (b) $m = 3$ (c) $m = 4$ are used in the experiment.

Table 2. The inversion result of the charge quantity of each particle in the multi particles based on experimental data.

		m=2			*m*=3			*m*=4		
rad	mm / pC	Δ=0	Δ=5	Δ=10	Δ=0	Δ=5	Δ=10	Δ=0	Δ=5	Δ=10
γ =0	7	7.18,7.23	8.71,5.6	9.53,4.44	6.77,6.63,7.31	8.25,5.64,8.34	8.93,8.95,4.94	7.29,7.27,7.3,6.69	7.93,8.15,7.98,5.9	5.38,8.59,8.62,5.52
	14	14.34,13.84	10.92,17.38	8.92,19.06	13.4,13.3,13.31	16.59,16.61,16.41	9.89,17.98,17.9	13.69,14.56,13.53,13.72	16.55,11.84,11.79,11.79	10.82,10.85,10.89,17.11
	22	21.6,22.76	26.81,17.36	30.22,13.97	20.91,21.18,20.96	18.13,26.11,18.15	28,28.24,15.9	21.02,21.26,22.87,22.96	18.61,25.35,18.4,18.84	17.29,16.78,27.2,16.54
	29	28.66,29.3	35.02,36.16	39.45,18.36	27.7,27.91,27.72	34.49,33.9,34.13	37.49,37.24,36.88	28.03,30.43,27.91,30.16	33.27,24.66,33.86,33.67	35.65,21.74,22.46,21.9
	37.5	37.12,38.34	45.34,45.02	51.59,51.61	39.9,39.64,39.32	44.63,44.34,45.08	27.06,26.89,48.38	35.57,38.69,36.01,39.21	31.63,31.74,42.93,31.71	28.46,29.89,28.98,29.41
γ =0.0873	7	7.12,6.92	5.24,5.34	4.17,9.89	7.1,7.14,7.14	6.32,7.89,7.96	5.68,8.39,5.61	7.55,6.67,7.41,6.71	6.08,8.03,7.77,6.04	4.19,9.85,9.84,4.19
	14	13.71,14.21	10.74,17.29	8.29,19.61	13.67,13.66,13.7	15.92,12.41,15.64	17.01,11.37,16.87	14.14,13.83,13.71,13.46	12.03,12.21,11.88,12.14	19.71,19.74,19.96,8.37
	22	21.84,22.42	26.57,27.22	13.07,13.05	22.59,22.51,21.54	24.53,25.08,24.6	17.57,17.27,26.44	22.04,23.15,22.91,22.96	18.96,18.76,19.34,18.83	13.25,30.75,12.9,13.31
	29	28.42,29.55	22.64,35.11	17.17,17.44	29.11,28.35,28.4	25.02,32.44,25.54	34.29,23.3,23.07	26.59,27.56,27.89,28.03	25.22,32.53,24.9,32.9	40.69,40.61,17.41,17.52
	37.5	36.89,36.85	46.09,45.77	22.16,21.94	35.85,36.65,38.63	32.79,33.23,32.99	45.52,45.08,30.33	38.38,36.17,38.88,36.04	43.09,32.04,31.26,42.84	22.44,52.35,23.76,21.82
γ =0.2618	7	6.89,6.87	4.52,4.59	10.5,10.66	6.71,7.33,6.73	8.28,8.34,8.29	4.17,4.1,4.15	6.82,7.24,7.27,6.77	8.46,8.59,5.57,5.52	10.41,3.57,3.58,3.61
	14	14.26,14.2	8.96,9.02	21.48,6.67	13.45,14.48,13.38	11.39,11.13,16.58	8.33,19.51,8.41	13.56,13.5,13.49,13.48	16.92,17.02,10.75,17.1	7.35,7.18,7.27,20.75
	22	21.5,22.53	29.17,14.35	10.36,10.48	20.86,20.92,21.08	25.92,18.31,26.14	13.08,13.42,30.88	23.05,22.95,21.16,21.21	17.11,17.5,27,26.77	11.04,32.65,32.75,11.03
	29	28.49,28.74	38.51,38.67	14.25,44.17	29.98,27.9,30.2	23.76,24.07,23.65	40.46,41.12,40.75	27.52,27.82,27.91,30.18	22.67,22.95,34.53,22.78	14.63,43.06,14.66,43.11
	37.5	38.33,38.68	50.36,25.16	17,17.82	35.97,36.06,39.01	44.77,44.51,30.78	22.27,22.48,52.54	36.35,38.72,38.87,36.02	45.79,29.14,29.09,29.41	19.01,18.62,18.88,56.13
γ =0.4363	7	7.14,7.07	4.77,9.15	10.63,10.74	7.31,6.64,6.7	8.32,5.62,8.3	9.48,4.36,9.71	6.72,6.66,7.21,7.27	8.86,8.81,4.9,8.74	4.49,4.35,9.52,9.58
	14	13.73,13.56	18.39,18.51	6.42,21.72	14.6,14.6,13.46	16.66,16.64,11.44	19.26,8.67,19.29	13.53,14.51,13.53,13.39	10.5,10.47,10.59,17.97	8.49,19.1,19.31,19.21
	22	22.62,21.56	28.58,28.7	33.3,10.85	22.85,22.86,21.11	17.91,17.87,17.71	13.55,13.84,30.56	21.17,20.93,21.16,22.7	16.12,16.29,27.63,27.25	30.02,13.73,30.11,29.9
	29	28.7,29.36	38.09,20.15	14.22,14.22	27.79,30.2,30.32	34.51,34.34,34.65	40.09,18.81,18.57	28.04,29.86,27.76,27.91	36.49,36.43,22.15,37.01	19.32,39.58,39.69,40.25
	37.5	38.29,36.58	25.98,25.76	18.67,55.64	39.07,38.81,39.07	44.62,44.5,44.44	51.8,52.37,23.85	35.93,38.35,35.94,36.16	46.74,27.76,28.08,46.52	22.21,23.45,23.15,51.43
γ =0.6109	7	7.2,7.14	8.86,8.91	10.04,9.88	6.76,7.25,7.38	8.08,5.86,5.75	4.59,4.64,9.24	6.84,6.57,6.77,7.23	8.31,8.32,8.26,8.38	9.91,9.73,4.09,9.8
	14	14.16,13.93	9.98,17.73	19.74,20.33	15.06,13.23,13.64	16.22,15.87,11.7	18.49,9.27,18.99	13.51,13.65,14.5,13.52	11.62,11.51,16.48,16.48	19.79,7.97,8.2,19.8
	22	21.49,21.51	16.29,27.86	12.96,12.22	20.86,22.96,21.14	18.51,25.32,24.85	14.19,14.42,14.45	22.82,21.43,22.86,21.34	26.01,25.83,25.99,25.46	31.15,31.25,31.18,12.7
	29	28.43,30.03	21.24,36.81	15.65,41.39	27.78,27.61,27.52	24.42,33.77,24.52	19.46,19.29,18.9	30.24,28.46,29.75,30.01	34.52,23.87,34.16,34.08	41.08,41.09,41.01,41.18
	37.5	37.55,37.45	27.47,27.25	20.96,21.74	38.08,36.11,39.36	42.97,31.41,43.06	51.07,24.19,24.68	36.37,38.94,36.19,36.12	43.88,44.28,44.35,30.29	21.93,21.84,53.05,21.8
γ =0.7854	7	7.45,6.82	5.48,5.55	9.56,9.6	7.27,6.71,7.26	5.85,8.06,5.87	4.99,4.97,5.02	6.78,7.3,7.29,6.78	5.59,5.69,5.51,5.63	8.41,5.6,5.57,5.62
	14	14.23,13.9	11.07,17.07	8.58,8.75	14.08,13.47,14.42	16.11,16.49,16.26	9.99,18.12,17.86	13.72,13.56,14.43,14.59	16.76,16.83,17.07,11.15	11.13,16.75,11.21,11.18
	22	22.21,23.09	26.78,27	29.94,13.58	23.32,22.81,22.84	25.53,18.27,25.54	15.92,28.42,28.61	20.94,22.94,21.25,21.16	26.33,17.65,25.74,17.75	17.82,17.53,17.33,26.48
	29	28.2,27.94	22.73,22.99	39.82,17.88	27.12,27.89,27.83	24.28,24.51,24.32	20.4,20.52,37.27	27.56,30.41,27.83,29.97	34.66,23.53,23.54,23.37	34.73,23.09,34.84,34.94
	37.5	38.14,36.9	45.67,45.65	22.9,51.15	38.28,38.89,35.79	31.18,43.25,43.55	26.38,27.24,48.66	38.67,38.06,38.8,36.19	45.03,45.59,45.04,29.79	29.68,30.06,30.54,44.83

charge quantity of each particle in the experiments, and what is filled in the cell is the charge quantity carried by each particle obtained by the inversion. By the way, the experiment carried out in this research can be numbered as a total of 54 experiment rounds. When $m = 2$, $\Delta = 0$ mm, and $\gamma = 0$ rad, the repeated experiments of changing the voltage are the first round of experiments, and the 54th round of experiments is repeated experiments under the condition of $m = 4$, $\Delta = 10$ mm, and $\gamma = 0.7854$ rad. Therefore, in Fig. 13, the experiment rounds from 1 to 6 refer to the repeated experiment of 6 rounds in which γ increases from 0 to 0.7854 rad in sequence when $m = 2$ and $\Delta = 0$ mm. Fig. 13 is a histogram of the estimated mean absolute error of the charge quantity of particles in each experiment round. Moreover, the mean absolute error of every 6 experiment rounds (the Δ of the 6 experiment rounds is the same) is marked in Fig. 13 in the form of text.

It can be seen from Fig. 12 that when Δ and m are the same, changing the value of γ does not affect the accuracy of the position inversion. This shows that the rotational symmetry of ESCA makes it possible to eliminate the influences of relative rotation of particles. When keeping m and γ constant, increasing Δ will significantly increase the error rate. This can also be explained, partly because the sensitivity of ESCA changes drastically in the radial direction. When Δ increases, the particle is closer to the center of the sensor, and its relative position with respect to the different electrodes is not much different, which cannot provide significant differentiated feature information, resulting in that it cannot be significantly distinguished by the proposed method, and this will affect the process of distinguishing the remaining particles. When only m increases, the error rate slightly increases. The reason is that the useful information of discrete points used to describe a single particle decreases, and the random error increases.

Figure 13 shows that the distribution of errors in the estimation of particles charge quantity based

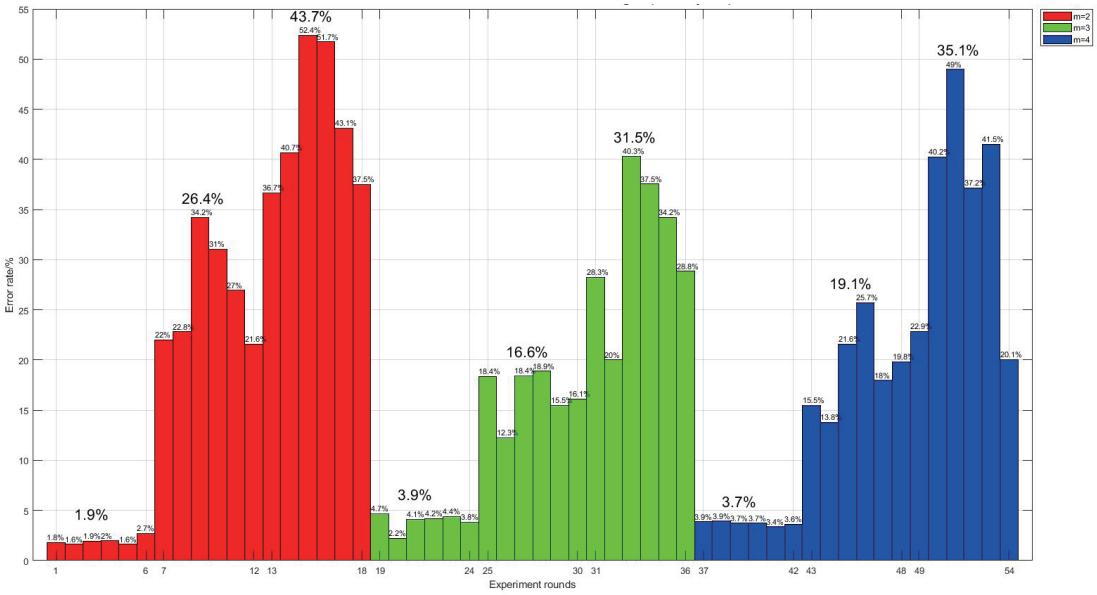

Figure 13. The estimated average error of the charge quantity of each particle in each experimental round.

on experimental data using the inversion method in this paper is consistent with the position inversion error. However, there is a difference that the error of the charge quantity inversion comes from the error transmission of small errors of the total charge quantity estimation, inevitable random errors in the measurement of induced charge quantity by electrodes, and the errors of the position inversion which is greatly affected by Δ changes. Especially, when Δ is equal to 0, the error of charge quantity inversion is less than 4.7%.

In general, the algorithm proposed in this paper can obtain accurate spatial positions and charge quantity of multiple particles located close to the wall of the flow channel but far from the center of the flow channel.

6. CONCLUSION

The inversion of the charge quantity and spatial position of charged particles in the oil line and gas path are very practical. When ESCA is used in an aero-engine oil line, it directly monitors the charge quantity of the wear debris which is the link between the physical properties of the debris and the state of friction and wear. Only by accurately obtaining the charge quantity of the particles can the wear state of the lubricating parts be accurately judged. This is the key technology for applying electrostatic sensors to the PHM of large mechanical systems. Moreover, the estimation of the spatial position of the particles can reflect the movement state of the particles in the oil, and the flow characteristics of the oil are beneficial to the improvement of the monitoring characteristic parameters of the electrostatic monitoring, and these will help to study the follow-up phenomenon of different particles in the oil flow then realize the identification of particle composition.

When ESCA is installed in the intake of aero-engine, the estimation of the total charge of the inhaled particle clusters, the charge quantity of each particle, and the position distribution of the particle clusters will be helpful to evaluate the damage level of the inhaled particles. Using ESCA to detect gas path debris in the exhaust of aero-engine can significantly improve the problem that the typical electrostatic monitoring mode only uses a single electrode to acquire sensing signals for monitoring, but cannot penetrate into the dimension of the induced particles information and resulting in high false alarm and missing alarm rates. In other words, applying the method proposed in this paper is promising to significantly reduce the false alarm rate and missing alarm rate of electrostatic monitoring.

This paper designs an ESCA applied to electrostatic monitoring. Based on the ESCA measurement model, its sensing mathematical model and finite-element simulation model are established to clarify the sensing characteristics of ESCA. A CS-based array signal processing method was developed, which clarified the specific method of multiple particles spatial position and charge quantity estimation. Furthermore, an experimental device that uses multi-charged oil droplets to simulate the situation of multiple particles passing through the flow channel was designed, and an experiment was carried out to simulate the passage of multiple particles at multiple different positions by adjusting the relative position of the sensor and the oil droplets generator. Based on experimental data and simulation data, it is verified that the proposed algorithm can accurately inverse the total charge quantity of multiple particles, the spatial position and the charge quantity of each particle of multiple particles distributed near the flow channel. With analyzing the error results, it is believed that the local refinement of the vicinity of the electrodes needs to be considered when constructing the sensing matrix is one of the effective means to reduce errors. Subsequent research will be expanded from improving the number of identifiable multiple particles to the practical application of the proposed multiple particles information inversion algorithm in the actual aero-engine oil line and gas path. On the other hand, the investigation on the effect of the number of electrode sensors on inversion results will be carried out in future. Finally, the deduction method of accurate particle size will be further studied.

ACKNOWLEDGMENT

This work was supported by the National Natural Science Foundation of China (Grant No. U1933202 and No. U1733201) and Foundation of Graduate Innovation Center in Nanjing University of Aeronautics and Astronautics (Grant No. kfjj20200723).

REFERENCES

1. Wen, Z., J. Hou, and J. Atkin, "A review of electrostatic monitoring technology: The state of the art and future research directions," *Progress in Aerospace Sciences*, Vol. 94, 1–11, 2017.
2. Couch, R. P. and D. R. Rossbach, "Sensing jet engine performance and incipient failure with electrostatic probes," *DTIC Document*, 1972.
3. Rosenbush, D. M. and R. P. Couch, "Electrostatic engine diagnostics with acceleration related threshold," U.S. Patent, 1986.
4. Powrie, H., K. McNicholas, "Gas path condition monitoring during accelerated mission testing of a demonstrator engine," *The 33rd AIAA/ASME/SAE/ASEE Joint Propulsion Conference and Exhibit*, 2904, 1997.
5. Powrie, H., J. Worsfold, "Gas path debris monitoring for heavy-duty gas turbines-a pilot study," *IDGTE Gas Turbine Symposium*, 168–179, 2001.
6. Angello, L., "Combustion turbine electrostatic debris monitoring system (EDMS) assessment, electric power research institute EPRI," *Tech. Rep.*, 2004.
7. Powrie, H., R. Wood, T. Harvey, L. Wang, S. Morris, "Electrostatic charge generation associated with machinery component deterioration, In Proceedings," *IEEE Aerospace Conference*, Vol. 6, 6-6, 2002.
8. Lin, J., Z. S. Chen, Z. Hu, Y. M. Yang, and X. Tang, "Analytical comparisons of electrostatic sensors with various geometric probes for gas path monitoring," *2014 Prognostics and System Health Management Conference (PHM-2014 Hunan)*, 1–5, 2014.
9. Chen, Z. S., X. Tang, Z. Hu, and Y. M. Yang, "Investigations into sensing characteristics of circular thin-plate electrostatic sensors for gas path monitoring," *Chinese Journal of Aeronautics*, Vol. 27, No. 4, 812–820, 2014.
10. Xu, C., J. Li, H. Gao, S. Wang, "Investigations into sensing characteristics of electrostatic sensor arrays through computational modelling and practical experimentation," *Journal of electrostatics*, Vol. 70, No. 1, 60–71, 2012.

11. Krabicka, J. and Y. Yan, "Finite-element modeling of electrostatic sensors for the flow measurement of particles in pneumatic pipelines," *IEEE Transactions on Instrumentation and Measurement*, Vol. 58, No. 8, 2730–2736, 2009.
12. Wang, L. J. and Y. Yan, "Mathematical modelling and experimental validation of electrostatic sensors for rotational speed measurement," *Measurement Science and Technology*, Vol. 25, No. 11, 115101, 2014.
13. Zhang, S., Y. Yan, X. C. Qian, and Y. H. Hu, "Mathematical modeling and experimental evaluation of electrostatic sensor arrays for the flow measurement of fine particles in a square-shaped pipe," *IEEE Sensors Journal*, Vol. 16, No. 23, 8531–8541, 2016.
14. Tasbaz, O. D., R. J. K. Wood, M. Browne, H. E. G. Powrie, and G. Denuault, "Electrostatic monitoring of oil lubricated sliding point contacts for early detection of scuffing," *Wear*, Vol. 230, No. 1, 86–97, 1999.
15. Powrie, H. E. G., C. E. Fisher, O. D. Tasbaz, and R. J. K. Wood, "Performance of an electrostatic oil monitoring system during an FZG gear scuffing test," *Proceedings of the International Conference on Condition Monitoring*, 145–155, 1999.
16. Powrie, H. E. G., "Use of electrostatic technology for aero engine oil system monitoring," *2000 IEEE Aerospace Conference Proceedings*, Vol. 6, 57–72, 2000.
17. Powrie, H. E. G. and C. E. Fisher, "Engine health monitoring: Towards total prognostics," *1999 IEEE Aerospace Applications Conference Proceedings*, Vol. 3, 11–20, 1999.
18. Mao, H. J., "Research on key technologies of health management of lubricating oil system and its lubrication parts," unpublished doctoral dissertation.
19. Tang, X., Z. S. Chen, Y. Li, and Y. M. Yang, "Compressive sensing-based electrostatic sensor array signal processing and exhausted abnormal debris detecting," *Mechanical Systems and Signal Processing*, Vol. 105, 404–426, 2018.
20. Donoho, D. L., "Compressed sensing," *IEEE Transactions on Information Theory*, Vol. 52, No. 4, 1289–1306, 2006.
21. Candès, E. J., "Compressive sampling," *Proceedings of the International Congress of Mathematicians*, Vol. 3, 1433–1452, 2006.
22. Candès, E. J. and T. Tao, "Near-optimal signal recovery from random projections: Universal encoding strategies," *IEEe Transactions on Information Theory*, Vol. 52, No 12, 5406–5425, 2006.
23. Wang, C., S. Zhang, Y. Li, and L. Jia, "Optimization of ESA for velocity distribution measurement based on cross-correlation sensitivity weighting method," *Process 2019 IEEE International Instrumentation and Measurement Technology Conference*, 1–6, 2019.
24. Armour-Chelu, D. I., S. R. Woodhead, and R. N. Barnes, "The electrostatic charging trends and signal frequency analysis of a particulate material during pneumatic conveying," *Powder Technology*, Vol. 96, No. 3, 181–189, 1998.
25. Hussain, T., W. Kaialy, T. Deng, M.S. Bradley, A. Nokhodchi, and D. Armour-Chélu, "A novel sensing technique for measurement of magnitude and polarity of electrostatic charge distribution across individual particles," *International journal of pharmaceutics*, Vol. 441, No. 1–2, 781–789, 2013.
26. Dunn, J. C., "A fuzzy relative of the ISODATA process and its use in detecting compact well-separated clusters," *Journal of Cybernetics*, Vol. 3, No. 3, 32–57, 1973.
27. Mao, H. J., H. F. Zuo, H. Wang, Y. B. Yin, and X. Li, "Debris recognition methods in the lubrication system with electrostatic sensors," *Mathematical Problems in Engineering*, 2018.
28. Mao, H. J., H. F. Zuo, W. J. Huang, Y. B. Yin, and C. N. Liu, "Mathematical modeling and calibration experiment of new electrostatic sensor in aviation," *Acta Aeronautica et Astronautics Sinica*, Vol. 37, No. 7, 2242–2250, 2016.
29. Huang, W. J., "Study on technologies of in-line electrostatic abrasive monitoring and distinguishing in oil system," unpublished doctoral dissertation.